Figure 3. *a*, Raman spectra of aqueous solution of CV only. Condition: [CV] = 10^{-8} mol dm^{-3}; *b*, Raman spectra of CV adsorbed on 50 nm particle without treatment with NaCl; *c–f*, Single-molecule SERS spectra of CV adsorbed on the particles of 50 nm at various times on treatment with NaCl. Condition: [CV] = 10^{-10} mol dm^{-3}, [NaCl] = 0.01 mol dm^{-3}.

According to the Otto and Person models, to have single-molecule SERS, there should be extensive coupling between the adsorbed molecule and metallic surface[15]. This is possible due to increase in the Fermi energy level of the metal in the nano stage. This causes a decreased energy gap between the Fermi level of the nanoparticles and LUMO of the adsorbed molecules. Thus, at a certain level of Fermi energy, the HOMO–LUMO energy separation resonates with the Fermi level and respond to SERS. This effect is much more pronounced in the case of the reported 'core–shell' structures of 50 nm.

1. Moerner, W. E. and Orrit, M., Illuminating single molecules in condensed matter. *Science*, 1999, **283**, 1670–1676.
2. Xie, X. S. and Trautman, J. K., Optical studies of single molecules at room temperature. *Annu. Rev. Phys. Chem.*, 1998, **59**, 441–480.
3. Fleischmann, M., Hendra, P. J. and McQuillan, A. J., Raman spectra of pyridine adsorbed at a silver electrode. *Chem. Phys. Lett.*, 1974, **26**, 163–166.
4. Moskovits, M., Surface-enhanced spectroscopy. *Rev. Mod. Phys.*, 1985, **57**, 783–826.
5. Campion, A. and Kambhampati, P., Surface-enhanced Raman scattering. *Chem. Soc. Rev.*, 1998, **27**, 241–250.
6. Frens, G., Controlled nucleation for the regulation of the particle size in monodisperse gold suspensions. *Nature*, 1972, **241**, 20–22.
7. Mallik, K., Mandal, M., Pradhan, N. and Pal, T., Seed mediated formation of bimetallic nanoparticles by UV irradiation: A photochemical approach for the preparation of 'core-shell' type structure. *Nano Lett.*, 2001, **1**, 319–322.
8. Wang, H., Lu, L., Zhou, Y., Xi, S., Zhang, H., Hu, J. and Zhao, B., Seed-mediated growth of large, monodisperse core–shell gold–silver nanoparticles with Ag-like optical properties. *Chem. Commun.*, 2002, 144–145.
9. Jana, N. R., Gearheart, L. and Murphy, C. J., Evidence for seed-mediated nucleation in the chemical reduction of gold salts to gold nanoparticles. *Chem. Mater.*, 2001, **13**, 2313–2322.
10. Bohren, C. F. and Huffmann, D. F., *Absorption and Scattering of Light of Small Particles*, Wiley, New York, 1983, pp. 183–188.
11. Emory, S. R., Haskins, W. E. and Nie, S., Direct observation of size-dependent optical enhancement in single metal nanoparticles. *J. Am. Chem. Soc.*, 1998, **120**, 8009–8010.
12. Krug, II, J. T., Wang, G. D., Emory, S. R. and Nie, S., Efficient Raman enhancement and intermittent light emission observed in single gold nanocrystals. *J. Am. Chem. Soc.*, 1999, **121**, 9208–9214.
13. Michaels, A. M., Nirmal, M. and Brus, L. E., Surface enhanced Raman spectroscopy of individual Rhodamine 6G molecules on large Ag nanocrystals. *J. Am. Chem. Soc.*, 1999, **121**, 9932–9939.
14. Hildebrandt, P. and Stockburger, M., Surface-enhanced resonance Raman spectroscopy of Rhodamine 6G adsorbed on colloidal silver. *J. Phys. Chem.*, 1984, **88**, 5935–5944.
15. Michaels, A. M., Jiang, J. and Brus, L., Ag nanocrystal junctions as the site for surface-enhanced Raman scattering of single Rhodamine 6G molecules. *J. Phys. Chem. B*, 2000, **104**, 11965–11971.
16. Schneider, S., Grau, H., Halbig, P., Freunscht, P. and Nickel, U., Stabilization of silver colloids by various types of anions and their effect on the surface-enhanced Raman spectra of organic dyes. *J. Raman Spectrosc.*, 1995, **27**, 57–68.
17. Nie, S. and Emory, S. R., Probing single molecules and single nanoparticles by surface-enhanced Raman scattering. *Science*, 1997, **275**, 1102–1106.

On the role of environment on corrosion resistance of the Delhi iron pillar

S. Halder, G. K. Gupta and R. Balasubramaniam*
Department of Materials and Metallurgical Engineering, Indian Institute of Technology, Kanpur 208 016, India

The total wetting time of the Delhi iron pillar due to rainfall and atmospheric conditions has been estimated. The wetting of the Delhi iron pillar due to environmental conditions was estimated by applying a non-steady state heat-transfer mathematical model. The estimated wetting times due to environmental conditions were two orders of magnitude lower than due to rainfall. The predicted wetting times were used to estimate the anticipated rust thickness on the surface of the Delhi iron pillar. This was much higher than the actual rust thickness on the pillar. Therefore, the importance of the protective passive film mechanism of

*For correspondence. (e-mail: bala@iitk.ac.in)

corrosion resistance of the Delhi iron pillar has been emphasized. The mild environment of Delhi is a contributing factor, but not the sole factor for the excellent corrosion resistance of the pillar.

THE Delhi iron pillar is one of the finest examples of utilization of skilled metallurgical manufacturing technologies in ancient India[1]. It is composed of wrought phosphoric iron, which has successfully stood the test of atmospheric corrosion[1]. It has been recently proved[2], using modern characterization techniques[3], that the remarkable atmospheric corrosion resistance is due to the formation of a protective passive film on the surface of the pillar, which has the ability of self-healing[4]. The general consensus is that the environment of Delhi is also conducive to the corrosion resistance of the pillar[5,6]. The large mass of the pillar has also been cited as a contributing factor to its corrosion resistance[7,8], based on the assumption that the pillar heats up relatively faster, thereby preventing long moisture residence times on the surface. It is well known that the presence of an electrolyte is one of the important requirements for the progress of corrosive attack. Therefore, the relatively low-humidity environment[5,6] coupled with the large mass of the pillar[7,8] has been cited as the primary reason for its excellent atmospheric corrosion resistance. The role of the environment of Delhi on the corrosion resistance of the pillar has not yet been addressed in a rigorous manner on a scientific basis. This important aspect will be explored in the present communication. The wetting time due to rainfall will be estimated utilizing time-averaged data for rainfall at New Delhi[6]. The recorded Delhi weather over a complete period of one year will be utilized in a model developed to estimate the wetting time of the pillar over this period. This will provide the wetting time due to low temperature and high humidity atmospheric conditions. The role of the environment of Delhi on the corrosion resistance of the pillar can be addressed more critically, based on the predicted wetting times.

Wranglen[6] provided the average data of atmospheric conditions of Delhi, which were collected over a period of 30 years between 1931 and 1960 (Figure 1). The average number of rainy days and the average rainfall for each month were provided. It is seen that Delhi receives its major rainfall in the monsoon season, which spans the months of July–September. In these three months, the recorded average humidity at Delhi (at 8:30 h) is higher than 70%. The total number of rainy days is approximately 37 and the total annual rainfall is about 690 mm, based on data from Figure 1. The rainy days are in the monsoon months and the total number of such days has been taken as 27. Based on the available data, it is difficult to assign the time period over which the pillar remains wet during these days. Taking a conservative estimate that the rainfall during these days occurs for only 6 h, the wetting time due to rainfall for the whole year is esti-

mated as approximately 160 h. This is a conservative estimate because only rainfall during the monsoon period was considered. Moreover, even for this monsoon season, only 6 h of rainfall was considered for each day. Whereas on all the 92 days in July–September, the humidity is higher than 70% at 8:30 am, only 27 days of 6 h of wetting per day has been considered as the actual wetting time.

The wetting time due to humidity and temperature conditions at Delhi will be estimated utilizing a mathematical model of heat-transfer on the surface of the pillar. The proposed heat-transfer model utilizes unsteady state heat-conduction phenomenon. Within the pillar body, heat will flow only by conduction, wherein the unsteady mode of heat-transfer must be considered because the temperature will vary as a function of time at any particular location inside the pillar due to the changing atmospheric conditions. Therefore, the recorded ambient atmospheric condition will be utilized in the analysis. The important variables that will be considered are ambient temperature, humidity and wind velocity. As heat from the ambient flows into or out of the pillar, the mode of heat flow between the ambient and the pillar occurs by all the three modes of heat-transfer, namely conduction, convection and radiation. However, conduction can be neglected compared to convection and radiation because conductive heat-transfer is
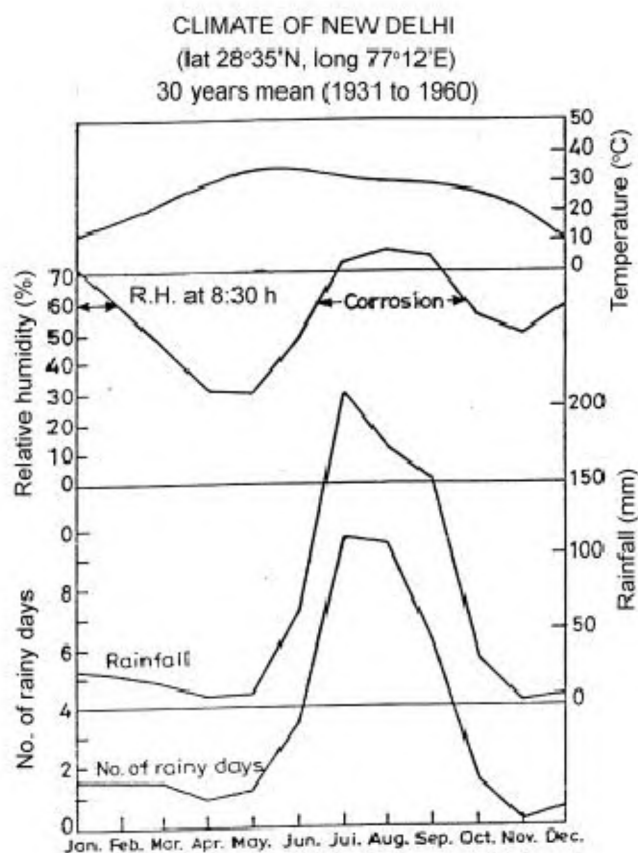

Figure 1. Atmospheric conditions at Delhi averaged over 30 years (1930–1960)[6].

usually insignificant when heat-transfer occurs across a solid–fluid interface[9]. The convective heat-transfer coefficient h is a sensitive parameter and changes with the geometry of the solid, fluid velocity and the thermo-physical properties of the fluid[9]. As it is variable in nature, it is difficult to use a standard value of h in the heat-transfer calculations. The variation of this parameter with the changing atmospheric conditions will also be considered in the model.

Another important parameter that will affect wetting time is the dew point, which is defined as the temperature below which water vapour in the ambient atmosphere will condense and form a thin film of water on the surface of the pillar. It is this thin moisture film which is responsible for corrosion. The moisture film enhances the anodic reaction (i.e. iron consumption), whose rate is strictly not constant during the wetting cycle but varies as a function of the wetting cycle[10–14] (Figure 2). The rate of anodic reaction is controlled by the rate of oxygen consumption (Figure 2). The surface moisture film will be present as long as the surface temperature of the pillar is below the dew point. The moisture film disappears when the surface temperature rises above the dew point, and corrosion stops. It is anticipated that significant wetting periods will occur during night when the ambient temperature is low and the humidity relatively high. The duration of the wetting period will vary with season. As stated earlier, in the monsoon season (three months between July and September in New Delhi), there is almost a continuous film of moisture during and after rains and wetting due to rainfall has been estimated as 160 h per year.

The following assumptions of the model are to be clearly understood.

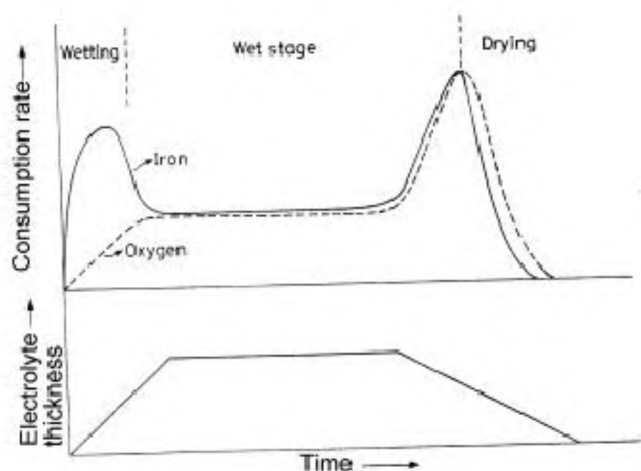1. The temperature, humidity and wind velocity conditions are assumed to be the same for all locations within Delhi. This is because the available meteorological data are for Delhi and not specifically at the location of the pillar.

2. The meteorological data were available only on an hourly basis for any given day. It has been assumed that atmospheric conditions do not change during a time interval of 60 min.

3. The pillar is taken to be an equivalent cylinder with a height of 6.19 m above the ground burial level, radius of 0.3735 m and volume of 0.7792 m^3 (Figure 3). This geometric equivalence, based on measured dimensions of the Delhi iron pillar[2,15], is necessary in order to simplify the mathematical formulations.

4. The heat flow between the pillar and the buried underground region has been neglected in order to simplify the model. This is reasonable as the area of the pillar exposed to the atmosphere is much larger than the area exposed to the soil.

5. Heat-transfer to and from the ambient environment is assumed to only occur on the lateral surface of the pillar that is above the ground. Moreover, the effect of surface films on heat-transfer has been neglected. Heat flow from the top surface of the pillar is neglected because its area is negligible compared to the lateral surface area. This assumption is also reason-
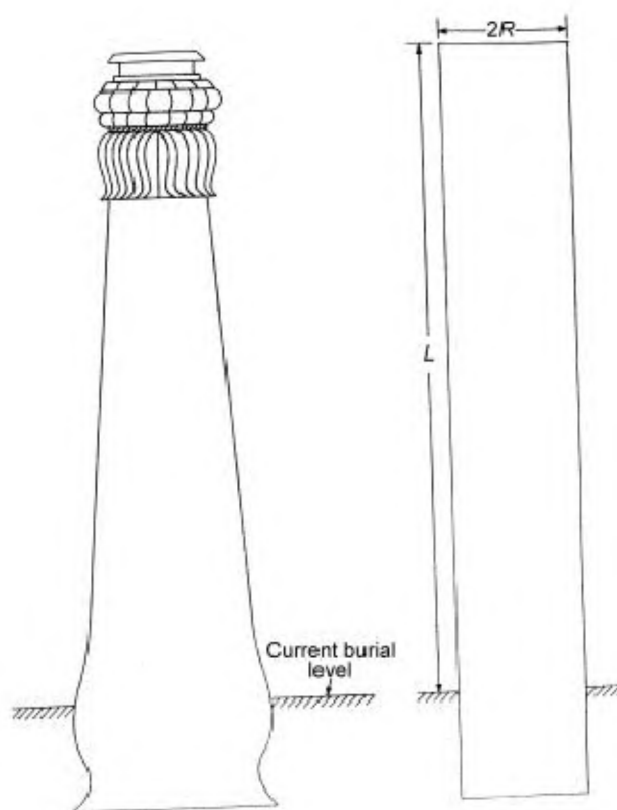

Figure 2. Schematic variation of corrosion rate of iron during each wetting cycle[11–14].

Figure 3. Relationship between Delhi iron pillar and simplified cylinder considered for use in the present analysis.

able because of the larger thermal resistance to heat flow in the axial direction compared to the radial direction[9].

6. Heat flows only in the radial direction and not in the axial or azimuthal (θ) direction, as the height of the pillar is significantly greater compared to its radius.

7. Convection and radiation will dominate heat-transfer between the surface of the pillar and the environment, while the heat-transfer within the pillar, will occur only by conduction.

8. The heat-transfer coefficient of air is dependent on ambient temperature, humidity and air velocity as the thermo-physical properties of air, like density, viscosity and specific heat capacity are dependent on these quantities[16].

9. The material of construction of the pillar is assumed to be wrought iron with the following thermo-physical properties[17]: density (ρ) 7700 kg/m^3; specific heat capacity (C_p), 481.16 J/kg-K and thermal conductivity (K), 58.938 W/m-K.

10. The average emissivity of wrought iron has been taken to be 0.65 (ref. 18) while estimating radiation heat flux between the surroundings and the pillar. It must be noted that the emissivity is a function of temperature and the surface finish. At 38°C, the emissivity for a polished wrought iron surface is 0.35, while that for a smooth surface 0.94 (ref. 18).

11. Meteorological data for the year 2001 were used and it is assumed that the climate of Delhi has not changed as a function of time. The estimated wetting time would, therefore, be a conservative estimate, because the phenomenon of global warming in recent years would provide higher surface temperature and hence lower wetting times.

12. The life of the Delhi iron pillar will be considered to be 1600 years in the environment of New Delhi. It is now known that the Delhi iron pillar was brought from Udayagiri in Central India to New Delhi in AD 1233 (ref. 1). The humidity levels at the original erection site in Udayagiri must have been higher than those at New Delhi, because the pillar was situated at a calculated astronomically significant location at Udayagiri (which lies exactly on the Tropic of Cancer) next to a large lake. Therefore, the estimated environmental wetting times in the present work are lower-bound values.

In order to obtain the surface temperature of the pillar as a function of time, it is adequate to solve the general heat-transfer conduction equation in the domain of the cylinder with the appropriate boundary conditions. The general conduction heat-transfer equation in r–ϕ–z cylindrical coordinates is given by:

$$K\left(\frac{\partial^2 T}{\partial r^2}+\frac{1}{r}\frac{\partial T}{\partial r}+\frac{1}{r^2}\frac{\partial^2 T}{\partial \varphi^2}+\frac{\partial^2 T}{\partial z^2}\right)+Q = \rho * C_p\left(\frac{\partial T}{\partial t}\right). \quad (1)$$

In eq. (1), K is the thermal conductivity of the pillar material, ρ is the density of pillar material, T is the temperature field at any instant of time, C_p is the specific heat capacity of the pillar material and Q is the heat generation term, which in the present case is zero as no heat is generated inside the pillar.

No heat flows in the z and ϕ directions, according to the assumptions. Therefore, the dependence of temperature on ϕ and z can be neglected. Equation (1) now simplifies to:

$$K\left(\frac{\partial^2 T}{\partial r^2}+\frac{1}{r}\frac{\partial T}{\partial r}\right)= \rho * C_p *\frac{\partial T}{\partial t}. \quad (2)$$

The above differential equation has a degree of two with respect to r and a degree of one with respect to t. Therefore, two boundary conditions and one initial condition are required to solve this equation. They are as follows:

(i) Boundary condition one:
   At $r = R$, heat flux $= h*(T_\infty - T_R)+ \sigma\varepsilon(T_\infty^4 - T_R^4)$,

where σ is Stefan–Boltzmann constant $(= 5.667*10^{-8}$ W/m^2-K$^4)$, ε is the emissivity, T_∞ is the ambient temperature and T_R is the instantaneous surface temperature.

(ii) Boundary condition two, based on the symmetry of the system:

   At $r = 0$, $\dfrac{\partial T}{\partial r} = 0$.

(iii) The initial condition:

   At $t = 0$, for $0 \le r \le R$, $T = T_{in}$,

where T_{in} is the initial temperature.

In order to solve the differential eq. (2), the finite difference method (FDM) was utilized[19]. In order to apply this powerful numerical procedure, the cylinder was divided into cylindrical elements, which have identical thickness equal to dr (Figure 4). By maintaining Fourier number $(\alpha*dt/dr^2)$ (where $\alpha= (K_{iron}/\rho_{iron}C_{p,iron})$) less than 0.5 for stability conditions[20], long computational times were avoided. Sixteen node surfaces, each surface corresponding to a surface of a cylindrical element, have been considered. The cylinder was divided into 15 equally spaced cylindrical elements. The first nodal surface was taken to be the outer surface of the pillar, while the 16th nodal surface was the central axis of the pillar (Figure 5).

As the heat-conduction is unsteady, all the calculations were performed in small time steps. For example, considering at $t = 0$, the temperature at a particular location is T within the pillar. In the next time step $(0 + \Delta t)$, the temperature of the same location may change to $T + \Delta T$. Therefore, the temperature profile in the pillar was estimated at each time step. In this regard, the fine distinc-

tion between time interval and time step needs to be emphasized. The time interval is the period during which the ambient conditions like temperature, humidity and wind velocity are assumed to be same throughout. It is 60 min in this case. However, the temperature at a particular location inside the pillar will change as a function of time within this time interval. The time interval (60 min) is, therefore, much longer compared to the time step. The time step adopted in this analysis is 1 s. At lower values of time step, refinement in the prediction of the temperature is obtained, however, entailing much longer computational times. The temperature variation at a particular
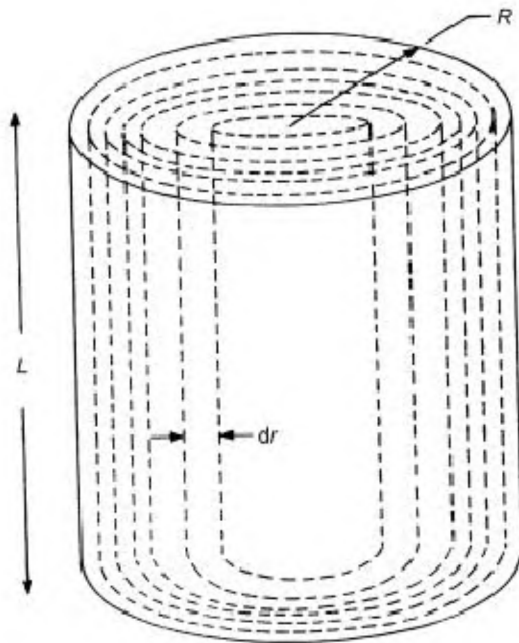

Figure 4. The FDM model considered division of the Delhi iron pillar equivalent cylinder into 15 finer cylindrical elements. A total of 15 fine cylinders were considered in the analysis.
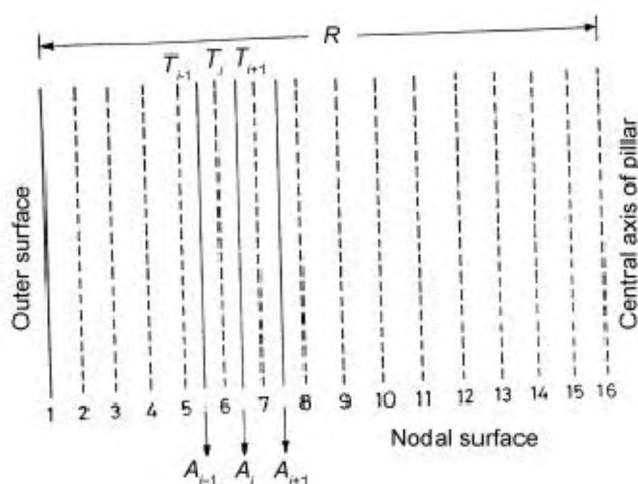

Figure 5. Schematic representation of the division of the pillar into segments for calculation purposes.

point, especially the surface, was estimated using the fixed convective boundary condition for the larger time interval. Within this time interval, the temperature at all points inside the pillar changes continually with time because of continuous conductive heat flow occurring in the pillar body.

The discretization of the heat-transfer equation for each element is realized in the form of a heat balance equation for each element (Figure 5). For all the nodal surfaces lying inside the pillar, i.e. nodal surfaces 2nd up to 15th, the heat balance equation is:

$$\frac{KA_i(T_{i-1,t}-T_{i,t})\mathrm{d}t}{\mathrm{d}r}+\frac{KA_{i+1}(T_{i+1,t}-T_{i,t})\mathrm{d}t}{\mathrm{d}r}$$
$$= \rho C_p V_i (T_{i,t+\mathrm{d}t}-T_{i,t}). \tag{3}$$

where A_i is the area of the ith nodal surface, A_{i+1} is the area of the $(i+1)$th nodal surface, $T_{i,t}$ is the temperature at the ith nodal surface at time instant t, $T_{i+1,t}$ is the temperature at the $(i+1)$th nodal surface at time instant t, $T_{i-1,t}$ is the temperature at the $(i-1)$th nodal surface at time instant t, and $T_{i,t+\mathrm{d}t}$ is the temperature at the ith nodal surface at time instant $t+\mathrm{d}t$. V represents the volume of the element enclosed by the $(i-1)$th and the ith nodal surfaces. The above equation states that the conduction heat flux entering a particular element is equal to the sum of the conduction heat flux leaving the element and the amount of heat which goes towards heating of the element.

In the special case of the first nodal surface, i.e. the outside surface of the pillar, the heat balance equation is:

$$hA_i(T_{\infty,t}-T_{i,t})\mathrm{d}t+\frac{KA_{i+1}(T_{i+1,t}-T_{i,t})\mathrm{d}t}{\mathrm{d}r}$$
$$+\sigma A_i(T_{\infty,t}^4-T_{i,t}^4)\mathrm{d}t = \rho C_p V_i (T_{i,t+\mathrm{d}t}-T_{i,t}). \tag{4}$$

Equation (4) states that the heat flux by convection and radiation from the ambient atmosphere to the first element is equal to the sum of the conduction heat flux leaving the first element and the heat needed to raise the temperature of the element by a finite amount. Similarly, for the 16th nodal surface, the heat balance equation is:

$$\frac{KA_{i-1}(T_{i-1,t}-T_{i,t})\mathrm{d}t}{\mathrm{d}r} = \rho C_p V_i (T_{i,t+\mathrm{d}t}-T_{i,t}). \tag{5}$$

Equation (5) states that the conduction heat flux through the innermost element is used up entirely to raise the temperature of the entire element.

The heat-transfer coefficient h is dependent on the thermophysical properties of air as well as ambient temperature (T_∞), per cent humidity (H) and air velocity (u). It can be estimated using the following correlation[9]:

$$\frac{hD}{K_{air}} = \left(0.3 + \frac{0.62 \, Re^{0.5} \, Pr^{1/3}}{(1 + (0.4/Pr)^{2/3})^{0.25}} \right) *$$
$$(1 + (Re/282000)^{5/8})^{0.8},$$

(6)

where $Re = \rho_{air} u D / \mu_{air}$ is the Reynolds number and $Pr = C_{p,air} \mu_{air}/K_{air}$ is the Prandtl number. D is the diameter of the pillar, ρ_{air} is the density, $C_{p,air}$ is the specific heat capacity, μ_{air} is the viscosity and K_{air} is the thermal conductivity of air. All these parameters depend on the ambient temperature (T_∞) and relative humidity (H).

The thermal conductivity of air is mildly dependent on the water content in the air. For the sake of simplicity, K_{air} has been taken to be a constant averaged value between that of dry air ($K = 0.0242$ W/m-K) and of water vapour ($K = 0.0261$ W/m-K). Therefore, the thermal conductivity of air was taken as 0.025 W/m-K.

The dependence of ρ_{air}, $C_{p,air}$, μ_{air} on T_∞ and H was estimated using a nonlinear regression model. Using a commercial software[16], the density, viscosity and partial pressure of water vapour in air were determined for several different combinations of T_∞ (ranging from 0 to 50°C) and H (ranging from 0 to 100%). The data were regressed to best fit a nonlinear equation with a high correlation coefficient. Further, the volume fraction of air and water vapour was obtained from the partial pressure, and then the mole fraction. These were used to obtain the C_p of moist air, basically dependent on T_∞ and H. The functional relationships of the above parameters, estimated by the Polymath software[21], are as follows:

$$\rho_{air}(\text{in kg/m}^3) = 2.3098 - 0.003867*T_\infty$$
$$+ 0.002598*H - 9.358*10^{-6}* T_\infty*H,$$

$$\rho_{air}/\mu_{air}(\text{s/m}^2) = 1.749*10^5 - 374.4748*T_\infty$$
$$+ 123.593*H - 0.44593*T_\infty*H,$$

$$C_{p,air} = C_{p,dry \, air}*(1 - m_{water \, vapour}) + C_{p,water \, vapour}*m_{water \, vapour},$$

where $m_{water \, vapour}$ is the mass fraction of water vapour in moist air and $C_{p,dry \, air}$ and $C_{p,water \, vapour}$ are 1006.43 and 2014 J/kg-K respectively. $m_{water \, vapour}$ can be calculated from the following expression,

$$m_{water \, vapour} = \frac{v_f * 18}{v_f * 18 + (1 - v_f) * 29},$$

where v_f is volume fraction of water vapour in air and 29 and 18 are molecular weights of air and water vapour respectively. v_f was calculated using the following expression.

$$v_f = \frac{pp_{water \, vapour}}{98723.2},$$

where $pp_{water \, vapour}$ is the partial pressure of water vapour in moist air and 98723.2 Pa is the mean atmospheric pressure at New Delhi. As New Delhi is situated at an altitude of 219 m from mean sea level, the mean atmospheric pressure value is less than 1 atm. The partial pressure of water vapour $pp_{water \, vapour}$ is dependent on T_∞ and H as given by:

$$pp_{water \, vapour} = -12.0076 + 0.08005*T_\infty$$
$$+ 4689.1473*H - 33.556*T_\infty*H - 1.329*10^{-4}*T_\infty^2$$
$$+ 0.06013 \, T_\infty^2*H.$$

In order to determine the time of wetting, the dew point at any instant is required. The dew point as a function of T_∞ and H is provided by[16,21]:

$$\text{Dew point (in K)} = 67.302 + 0.5634*T_\infty$$
$$+ 4.996*10^{-4}*T_\infty*H - 0.090225*H$$
$$- 28.97*\log_{10}H + 0.1931*T_\infty*\log 10 H$$
$$- 1.1*10^{-101}*10^H - 3.13*10^{-104}*10^H*T_\infty.$$

The meteorological data utilized were the ambient temperature, relative humidity and wind velocity conditions of New Delhi for the entire year 2001 (ref. 22). Each day in the year was divided into 24 time intervals of 1 h duration, during which the ambient temperature, humidity and wind velocity were assumed to remain the same. Separate data files were created for ambient temperature, humidity and wind velocity for all the days in the year. This operation was tedious as it involved analysis of a large database. In some cases, the data for some time intervals were not available, in which case intelligent extrapolations were made utilizing data for that particular time interval in the days just before and just after the day in the year for which the data were not available. This extrapolation was also confirmed by observing the general trend in variation of these parameters for other days of the month for which data were available.

The values of the ambient temperature, humidity and wind velocity were read from these files and fed into a computer program which calculated the total wetting time using the FDM procedure discussed earlier. The time step used in the program was 1 s. The surface temperature was calculated after every second for the entire time period of 1 year.

The functional relationships were used in the FDM model to first predict the temperature field inside the pillar as well as the temperature at the surface of the pillar after each time step. The calculations were performed in a Pentium-IV microprocessor-controlled computer. The surface temperature was calculated for every time step of 1 s using the above expressions. If the temperature of the surface in that particular time step moved below the dew point, 1 s was added to the total wetting time. The total wetting time was thus calculated by carrying out the above

Table 1. Estimated wetting times of the Delhi iron pillar due to environmental conditions at New Delhi in 2001

(2*R*, *L*)	Wetting time (s)											
	January	February	March	April	May	June	July	August	September	October	November	December
(0.35, 7.184)	3248	3600	0	0	0	0	0	0	0	0	0	0
(0.36, 6.74)	3449	3600	0	0	0	0	0	0	0	0	0	0
(0.37, 6.332)	3600	3600	0	0	0	0	0	0	0	0	0	0
(0.38, 5.956)	3600	3600	0	0	0	0	0	0	0	0	0	0
(0.39, 5.608)	3600	3600	0	0	0	0	0	0	0	0	0	0
(0.4, 5.2856)	3600	3600	0	0	0	0	0	0	0	0	0	0
(0.3735, 6.19) (actual)	3600	3600	0	0	0	0	0	0	0	0	0	0

procedure over all the time intervals spanning across the desired period of study.

The total wetting time as a function of the month of the year 2001 is presented in Table 1. Calculations were performed with the same time step of 1 s for seven differing radii of the pillar (0.35, 0.36, 0.37, 0.3735, 0.38, 0.39 and 0.40 m), maintaining the mass of the pillar constant. The emissivity was kept constant at 0.65. The results in Table 1 indicate almost constant wetting times with increasing radius.

The results for the Delhi iron pillar provide the total wetting time in one year (for $L = 6.332$ m, $R = 0.37$ m and $e = 0.65$) as approximately 2 h (Table 1). The wetting times obtained from the mathematical model must be considered as lower-bound values. First, it is to be noted that when the surface temperature exceeds the dew point, all the moisture previously present on the surface will not vaporize instantaneously, but will do so as a function of time because kinetics is also involved. Therefore, kinetics of drying and wetting needs to be considered in the estimation of wetting time as well. Moreover, the climate of Delhi is anticipated to be warmer nowadays compared to ancient times. Therefore, the total wetting times due to environmental conditions (2 h/year) are about two orders of magnitude lower than those due to rainfall. These estimated wetting times can be utilized to arrive at reasonable estimates for the expected corrosion of the pillar over its life period of 1600 years.

The total period of wetting of the pillar in electrolyte due to atmospheric moisture condensation, due to both environment and rainfall, is estimated as (162 h/year × 1600 years) 2,59,200 h or about 30 years. Assume now that during this period of 30 years, the pillar material (phosphoric wrought iron with entrapped slag particles) corroded at a rate provided by the flat plateau in the iron consumption rate of Figure 2. This implicitly means that the enhanced iron corrosion rates due to drying conditions (Figure 2) are neglected and here again the estimated corrosion depths will be lower-bound values. It is important to choose a reasonable value for corrosion rates for the plateau in the iron consumption rate. The aqueous corrosion rate of a piece of Delhi iron pillar was estimated in two solutions[23] and the rates were 28 μm/year in 0.001%

NaCl solution and 252 μm/year in 0.003% SO_2 solution. Therefore, the loss suffered by the wetting of the pillar for a period of 30 years must be between 840 and 7560 μm. This must convert to rust thickness of approximately 1680 to 15,120 μm. This is also in tune with the anticipated rust thickness from the known atmospheric corrosion rates of iron in several environments[24]: 4–45 μm/year in rural, 26–104 μm/year in marine, 23–71 μm/year in urban and 26–175 μm/year in industrial environments. Assuming the Delhi weather to be rural, the estimated corrosion product layer over a period of 1600 years should be between 6400 and 72,000 μm. This has certainly not been the situation in case of the Delhi iron pillar, because its surface does not show any evidence of significant rusting.

It must be noted that the above calculations did not consider the varying corrosion rate as a function of wetting cycle (Figure 2). Therefore, the use of steady-state corrosion rates of the Delhi pillar iron in mild NaCl and SO_2 solutions provides lower-bound values. It is now interesting to compare the actual measured values of the thickness of the films on the surface of the pillar. Bardgett and Stanners[8] measured the thickness of the Delhi pillar rust at two locations, on the polished band (which was present due to the habit of visitors trying to clasp their hands around the pillar) and in the upper regions of the pillar where the rust was relatively undisturbed. They reported the rust thickness as 50 μm in the polished region and 500–625 μm in the region above. The actual protective rust thickness on the Delhi iron pillar is, therefore, lower than that predicted by wetting due to rainfall and atmospheric conditions. The lower corrosion rate of the Delhi iron pillar must be due to the formation of a protective passive film on the surface at the interface between the metal and scale[2]. Therefore, the present analysis appears to validate the protective passive film theory of corrosion resistance of the Delhi iron pillar. The effect of the mild environment of Delhi is, nevertheless, a contributing factor, but not the sole factor as the present calculations have shown. The relatively large mass of the pillar is also a contributory factor.

The excellent corrosion resistance of the phosphoric iron of the Delhi iron pillar is obtained only for the case of mildly corrosive environments, like atmospheric expo-

sure. Had the pillar been completely immersed in a solution or in soil, the rate of corrosion of the Delhi pillar iron would have been comparable to modern iron and steels. This has been verified by corrosion studies on other ancient Indian phosphoric irons (for example, see ref. 25). The passive film prevents ingress of atmospheric corrosion due to the benign nature of the exposure environment.

The wetting time (due to rainfall and atmospheric conditions) of the Delhi iron pillar has been estimated for a period of one year. A non-steady state heat-transfer mathematical model has been applied to determine the wetting of the Delhi iron pillar based on environmental conditions. The estimated wetting times due to environmental conditions were two orders of magnitude lower than those due to rainfall. Based on the known wetting times, the anticipated film thickness on the surface of the Delhi iron pillar has been predicted, which is much higher than the actual rust thickness on the pillar. The importance of the protective passive film mechanism of corrosion resistance of the Delhi iron pillar has, therefore, been emphasized.

1. Balasubramaniam, R., *Delhi Iron Pillar: New Insights*, Indian Institute of Advanced Study, Shimla, 2002.
2. Balasubramaniam, R., On the corrosion resistance of the Delhi iron pillar. *Corros. Sci.*, 2000, **42**, 2103.
3. Balasubramaniam, R. and Ramesh Kumar, A. V., Characterization of Delhi iron pillar rust by X-ray diffraction, Fourier infrared spectroscopy and Mössbauer spectroscopy. *Corros. Sci.*, 2000, **42**, 2085.
4. Balasubramaniam, R., On the growth kinetics of the protective passive film of the Delhi iron pillar. *Curr. Sci.*, 2002, **82**, 1357.
5. Hudson, J. C., The Delhi iron pillar. *Nature*, 1953, **172**, 499.
6. Wranglen, G., The rustless iron pillar at Delhi. *Corros. Sci.*, 1970, **10**, 761.
7. Sanyal, B. and Preston, R., *Note on Delhi Pillar*, Chemical Research Laboratory, London, 1952.
8. Bardgett, W. E. and Stanners, J. F., Delhi iron pillar – A study of the corrosion aspects. *J. Iron Steel Inst.*, 1963, **210**, 3; *NML Tech. J.*, 1963, **5**, 24.
9. Holman, J. P., *Heat Transfer*, McGraw Hill, New York, 1997, 8th edn.
10. Evans, U. R. and Taylor, C. A. J., Mechanism of atmospheric rusting. *Corros. Sci.*, 1972, **12**, 227.
11. Stratmann, M., The investigation of the corrosion properties of metals covered with adsorbed electrolyte layers – a new experimental technique. *Corros. Sci.*, 1987, **27**, 869.
12. Stratmann, M. and Streckel, H., On the atmospheric corrosion of metals which are covered with thin electrolyte layers – I. Verification of the experimental technique. *Corros. Sci.* 1990, **30**, 681.
13. Stratmann, M. and Streckel, H., On the atmospheric corrosion of metals which are covered with thin electrolyte layers – II. Experimental results. *Corros. Sci.*, 1990, **30**, 697.
14. Stratmann, M. and Streckel, H., On the atmospheric corrosion of metals which are covered with thin electrolyte layers – III. The measurement of polarization curves on metal surfaces which are covered by thin electrolyte layers. *Corros. Sci.*, 1990, **30**, 715.
15. Balasubramaniam, R., New insights on the corrosion of the Delhi iron pillar based on historical and dimensional analysis. *Curr. Sci.*, 1997, **73**, 1057.
16. http://www.geocities.com/CapeCanaveral/Galaxy/4707/Aeronotes/ATMOprog.htm, November 2002.
17. ASM Metals Reference Book, 1993, 3rd edn, p. 152.
18. http://www.newportus.com/Products/Techncal/MetlEmty.htm, November 2002.
19. Sastry, S. S., *Introductory Methods of Numerical Analysis*, Prentice Hall of India Pvt Ltd, New Delhi, September 1999, 3rd edn.
20. Ghoshdastidar, P. S., *Computer Simulation of Flow and Heat Transfer*, Tata McGraw Hill, New Delhi, 1998, 1st edn.
21. http://www.polymath-software.com, November 2002.
22. http://www.underground.com, November 2002.
23. Ghosh, M. K., The Delhi iron pillar and its iron. *NML Techn. J.*, 1963, **5**, 31.
24. Leygraf, C., Atmospheric corrosion. In *Corrosion Mechanisms in Theory and Practice* (ed. Marcus, P.), Marcel Dekker, New York, 2002, 2nd edn, pp. 529–562.
25. Balasubramaniam, R. and Ramesh Kumar, A. V., Corrosion resistance of the Dhar iron pillar. *Corros. Sci.*, 2003, **45**, 2451.

Analysis of Cry2A proteins encoded by genes cloned from indigenous isolates of *Bacillus thuringiensis* for toxicity against *Helicoverpa armigera*

Shantanu Kumar[†], V. Udayasuriyan[#,*],
P. Sangeetha[#] and M. Bharathi[#]

[†]Centre of Advanced Studies in Agriculture Microbiology, and
[#]Centre for Plant Molecular Biology, Tamil Nadu Agricultural University, Coimbatore 641 003, India

The Cry2A proteins of *Bacillus thuringiensis* are promising candidates for management of resistance development in insects due to their differences from the currently used Cry1A proteins, in structure and insecticidal mechanism. The Cry2Aa and Cry2Ab proteins isolated from recombinant *Escherichia coli* strains harbouring indigenous *cry2Aa* and *cry2Ab* genes under the control of T7 promoter were tested for toxicity against *Helicoverpa armigera* (Hubner). In artificial diet bioassay, inclusions containing Cry2Aa and urea-solubilized Cry2Aa protein showed 100% mortality of *H. armigera* at a concentration of 650 and 100 ng ml^{-1} after 48 and 72 h respectively. On the other hand, the Cry2Ab protein inclusions as well as urea-solubilized Cry2Ab protein were not toxic to *H. armigera*, probably due to lack of solubility in alkaline condition and improper folding after urea solubilization.

BACILLUS thuringiensis (*Bt*) is a soil bacterium that produces one or more crystalline inclusion bodies containing specific insecticidal protein(s) or δ-endotoxin(s)[1]. The final toxicity of *Bt* is the result of a series of events, including solubilization of crystal, activation of protoxin by gut

---